Check for updates

Formulation and characterization of a sortase a inhibitor-loaded PMMA bone cement

Yin-Yu Qi,†[ab] Lu-Yang Han,†[ab] Long-Xu Han,†[a] Wen-Han Bu,[ab] Yang Xu [ID] *[ab] and Jian-Jun Chu*[ab]

A sortase A inhibitor (SrtA I)-loaded bone cement (SLBC) containing 1-(3,4-dichlorophenyl)-3-(dimethylamino)propyl-1-one hydrochloride (AEEK1) was reported. Compared with gentamicin-loaded bone cement (GS cement), which is a widely used antibiotic-loaded bone cement in cemented total joint replacement (TJR), SLBC demonstrated a significantly prolonged effective antibacterial duration against both *Staphylococcus aureus* (*S. aureus*) and methicillin-resistant *S. aureus* (MRSA). The quasi-static compressive strength, maximum polymerization temperature, and setting time of SLBC were within the limits stated in the ISO 5833 standard and comparable to the corresponding values of GS cement. *In vitro* and *in vivo* experimental results confirmed the biocompatibility of SLBC and showed its easy injectability into porcine T12 vertebrae. Taken together, these findings suggest that SLBC may have potential for managing/treating prosthetic joint infections, which is a common complication in cemented TJR.

1. Introduction

With factors such as global aging and war traumas, the number of total joint replacements (TJRs) is continuously increasing, with millions of cases occurring each year.[1,2] Periprosthetic joint infection (PJI) is a severe complication of TJR. In order to prevent PJI, antibiotic-loaded bone cement (ALBC) based on poly(methyl methacrylate) (PMMA) has been widely used.[3–12] Antibiotics work through their bacteriostatic or bactericidal properties. However, over the years, the bacteria commonly involved in PJI have developed resistance to antibiotics eluted from ALBCs.[13–16] Perhaps, the most well-known reason is the short effective elution period of antibacterial agents caused by the burst release of antibiotics, which is usually below the MIC after 1 week.[2] Furthermore, in recent literature, the "race to the surface" (the race between the formation of biofilm on the surface of an infected implant and the movement of an antibiotic to that surface) is usually won by the biofilm.[17–19] In other words, a biofilm forms quickly on the surface of the implant, preventing antibiotics eluted from agents such as ALBC from reaching the bacteria on that surface. A recent study has indicated that the inefficiency of ALBC in preventing PJI may be attributed to the aforementioned reasons.[3] It poses an imminent threat to the public health; hence, there is an urgent need for new strategies to combat antibiotic resistance.

Staphylococcus aureus (*S. aureus*) is the most common and destructive bacterium in PJI.[20,21] Sortase A (SrtA), as a biological anti-virulence target of *S. aureus*, holds promise for therapeutic intervention because inhibiting SrtA may not exert selective pressure on bacteria, thus avoiding the emergence of drug-resistant strains.[22–27] Therefore, SrtA inhibition appears to be an excellent anti-infection strategy.[28–32] Although a sufficient number of SrtA inhibitors (SrtA is) are currently known,[28,29] only a few of them have been studied *in vivo*, and the vast majority of inhibitors have not been clinically evaluated.[28,32] This indicates an urgent need to follow up on these potent inhibitors and translate them into tools available for clinical treatment to deal with PJI.

In the present study, we formulated an antibacterial bone cement, whose powder ingredients included a sortase A inhibitor, and determined a variety of its properties. The properties were antibacterial activity against *S. aureus* and MRSA (to highlight the antibacterial spectrum of the inhibitor), surface morphology of fracture specimens in SEM, radiopacity, quasi-static compression strength and modulus, *in vitro* cytotoxicity, *in vitro* hemolysis, toxicity in C57 mice, polymerization temperature, setting time, and injectability into porcine T12 vertebrae.

[a] Bengbu Medical University, The Second People's Hospital of Hefei (Affiliated Hospital), Anhui 230011, China. E-mail: chujianj@mail.ustc.edu.cn; xuyang@hfut.edu.cn

[b] Department of Pharmaceutical Science and Engineering, Hefei University of Technology, Hefei, Anhui 230009, China

† Yin-Yu Qi, Lu-Yang Han, Long-Xu Han contributed equally to this work.

2. Materials and methods

2.1 Materials

Poly(methyl methacrylate) and methacrylic acid (MMA) were purchased from Sigma-Aldrich Co., USA. Benzoyl peroxide

(BPO) and *N,N*-dimethyl-*p*-toluidine (DMPT) were purchased from J&K Science Co., Ltd, China. Barium sulfate (BaSO₄) was purchased from Shanghai Aladdin Bio-Chem Technology Co., Ltd. Gentamicin sulfate (GS) was purchased from Shanghai Macklin Biochemical Co., Ltd, China. The SrtA inhibitors used in this study were two aryl (β-amino)ethyl ketone (AAEK) compounds, namely 1-(3,4-dichlorophenyl)-3-(dimethylamino) propyl-1-one hydrochloride (AAEK1) and 3-dimethylamino-1-(thienyl)-propyl-1-one hydrochloride (AAEK2). 1-(3,4-Dichlorophenyl)-3-(dimethylamino)propyl-1-one hydrochloride was purchased from Shanghai Acmec Biochemical Technology Co., Ltd 3-Dimethylamino-1-(thienyl)-propyl-1-one hydrochloride was purchased from Bide Pharmatech Co., Ltd *Staphylococcus aureus* (*S. aureus* ATCC 25923) and a clinically isolated multiple-resistant *Staphylococcus aureus* (hereafter referred to as clinical MRSA or MRSA; this strain is resistant to methicillin, various other antibiotics, and GS; see SI Table S1 for details) were obtained from the Department of Clinical Laboratory, Second People's Hospital of Hefei. MC3T3-E1 cells and their specialized cell culture medium were purchased from Wuhan Servicebio Biotechnology Co., Ltd. SPF grade C57 mice and rabbit erythrocytes were provided by the Animal Experiment Center of Anhui Medical University. BPO was vacuum-dried at room temperature for 24 hours before use. PMMA was ground to a particle size of 80–100 mesh and used. Other chemicals require no further purification or treatment and can be used as received.

2.2 Preparation of bone cement

All bone cements used in this study were prepared according to the formulations described in Table 1 and Fig. 1, with the design closely approximating that of commercially available bone cement. Briefly, the antibacterial agent, as a component of the solid phase, was uniformly mixed with PMMA, BPO, and barium sulfate. Afterwards, the solid and liquid phases were mixed and stirred, and then injected into the mold for shaping.[33,34] Prior to preparing antibiotic-loaded bone cement, three antibacterial agents were separately mixed with the powder using standardized powder-blending protocols. After homogeneously mixing the powder and liquid phases of each bone cement group at ambient temperature (23 °C ± 1 °C), the mixtures were immediately transferred into poly-tetrafluoroethylene (PTFE) molds of specified dimensions for polymerization. Disk-shaped specimens (Ø 6 × 3 mm) were prepared for antibacterial property evaluation. Cylindrical

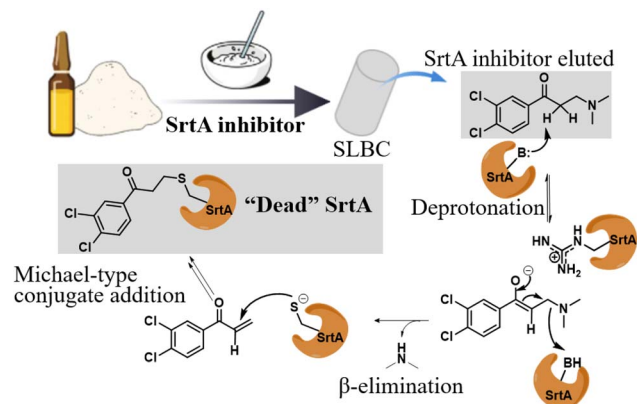**Table 1** Bone cement formulations and groupings (the total amount of bone cement is approximately 1 g)

Formulation	Powder (mg)				Liquid (µL)	
	PMMA	BPO	BaSO₄	Drug	MMA	DMPT
PMMA cement	525	13	100	0	379	7.5
5% AAEK1 cement	493.1	13	100	31.9	379	7.5
5% AAEK2 cement	493.1	13	100	31.9	379	7.5
5% GS cement	493.1	13	100	31.9	379	7.5

Fig. 1 Preparation of sortase A inhibitor-loaded bone cement (SLBC) and its antibacterial mechanism.

specimens (Ø 6 × 12 mm) were prepared for mechanical testing and hemolytic activity assessment, with extracts prepared for biocompatibility studies. Square-plate specimens (20 × 20 × 2 mm) were fabricated for scanning electron microscopy (SEM) analysis.

2.3 Preparation of cement extracts

After being sterilized by UV irradiation, cylindrical bone cement specimens from each group were immersed in physiological saline (0.9% NaCl solution) and in cell culture medium, according to GB/T 16886 standards, and the sample-to-liquid ratio was set at 0.2 g mL⁻¹. The saline groups were incubated at 37 °C in a 5% CO₂ atmosphere for 30 minutes, while the culture medium-treated groups were incubated under identical conditions for 24 hours. The saline extract of the bone cement obtained was used for the animal hemolysis test and acute toxicity test, and the cell culture medium extract was used for the *in vitro* cytotoxicity test.

2.4 Determination of antibacterial activity

S. aureus and clinical MRSA strains were resuscitated and sub-cultured, and bacterial suspensions were prepared at a concentration of 0.5 × 10⁸ CFU mL⁻¹ after three subcultures. A 100 µL aliquot of bacterial solution was pipetted and spread evenly on nutrient agar plates, and disc-shaped bone cement samples (UV irradiation for 30 min) were placed on each plate. The center-to-center distance between each cement sample was greater than 24 mm, and the distance between the sample and the edge of the plate was greater than 15 mm (S3). After marking, the plates were incubated at 37 °C in a 5% CO₂ incubator for 24 h, and the ring diameter of each cement inhibition zone was measured to evaluate its antibacterial activity. The plates were replaced daily with freshly coated plates, and specimens were transferred to new plates, and their locations were marked. The antibacterial properties of each group were tested continuously for 7 days.

In order to further improve clinical relevance, the surface antibacterial activity of bone cement after different soaking durations (0–5 days) was studied. Cement samples were soaked in a glass tube containing 1 mL of the bacterial solution

prepared above and incubated for 6 hours. Then, the samples were removed, the surface non-adherent bacteria were slowly washed off with normal saline, and then the rinsed samples were placed into a centrifuge tube containing 5 mL of normal saline. The tubes were vibrated in an ultrasonic shaker for 3 minutes, and the samples were removed. A 40 μL of the soni-cated liquid was pipetted and added to 4 mL of normal saline for dilution, and finally a pipette was used to aspirate 40 μL of the dilution for plate coating. After 24 hours of incubation in a constant-temperature incubator, colonies were counted, and the antibacterial rate was calculated. For each cement group, three specimens were used.

2.5 Characterization of bone cement (SEM and FT-IR)

Two batches of square-plate bone cement specimens were prepared for each group. After liquid nitrogen embrittlement, one batch was soaked in physiological saline at 24 °C ± 1 °C for 7 days, while the other batch was not soaked. The treated bone cement specimens were coated with gold particles in a sputter coater and characterized by scanning electron microscopy (SEM; JSM 6700, OLYMPUS, Tokyo, Japan) to analyze the cross-sectional morphology of the specimen before and after soaking for 7 days.

A small amount of bone cement powder was mixed with potassium bromide (KBr) at a ratio of about 1 : 50, ground into fine powder and pressed into transparent sheets. The functional groups of the composite materials were analyzed by Fourier transform infrared (FT-IR) spectroscopy in the frequency range of 4000–400 cm^{-1} using an FT-IR spectrometer (Bruker Vector-22). The FT-IR spectra were baseline-corrected and plotted using Origin Pro 2023 software.

2.6 Radiopacity

In this experiment, a CT scanner (SIEMENS SOMATOM AS 64-slice CT) was used to quantify the HU of the bone cement. Cylindrical bone cement (Ø 30 mm × 15 mm) was prepared, and five in each group were tested. Before scanning, the sample was completely immersed in a water mold filled with deionized water, and the CT scanning parameters were set as follows: tube voltage 120 kVp, B30f standard soft tissue algorithm, and layer thickness 1.0 mm. After acquiring the images, quantitative analysis was performed using specialized software (PACS system). On the axial images of each specimen, the central region of five consecutive layers was selected to place the circular region of interest (ROI) with a diameter of 20 mm to avoid edge area artifacts. The mean HU and standard deviation of the pixels within each ROI were recorded, and the final HU of each sample was calculated as the average of the ROI of the five consecutive layers. For each cement group, five specimens were tested.

2.7 Determination of quasi-static compressive properties

The quasi-static compressive strength and quasi-static elastic modulus of each group of bone cement were tested according to ISO5833. Two batches of cylindrical bone cement specimens were prepared for each group. One batch was soaked in

physiological saline at 24 °C ± 1 °C for 7 days, while the other batch remained unsoaked. The specimens were polished with 1000-grit sandpaper to ensure parallel upper and lower surfaces, and the weight was controlled at 0.4 ± 0.01 g. Quasi-static compression experiments were performed at 23 °C using a computer-controlled material testing machine (Bose company, USA) at a loading rate of 20 mm min^{-1}. The quasi-static compressive strength was obtained from the recorded stress–strain curve, and the modulus of elasticity is calculated from the linear slope of the stress–strain curve. In order to further explore other aspects of mechanical properties, we additionally prepared a long strip sample (75 × 10 × 3.3 mm) and carried out a three-point bending experiment according to ISO5833 to measure the quasi-static bending strength and bending modulus of the three types of bone cements. For each cement group, five specimens were tested.

2.8 Determination of cytotoxicity

Under sterile conditions at 37 °C and 5% CO_2, recovered cells were cultured using MC3T3-E1 cell-specific medium, and cells that had undergone three subcultures were selected for related experiments. Cells in the logarithmic growth phase were centrifuged after trypsin digestion, and then a diluted MC3T3-E1 cell suspension was seeded into wells of 96-well plates at approximately 5×10^3 cells per well. After microscopic obser-vation of cell attachment, the original medium was discarded, and 100 μL of cement medium extract (prepared as described above) was added to each well for co-culture with MC3T3-E1 cells.

On the first, third, and fifth days after cell co-culture, the CCK-8 reagent was mixed with medium at a 1 : 9 volume ratio. The original medium in the plate was discarded, and 100 μL of the mixed solution was added, followed by 2 hours of incuba-tion. The morphological changes of the cells were then observed using an inverted fluorescence microscope (Nikon DS-Fi3). The plates were placed in a microplate reader, and the wavelength was set to 450 nm to measure the optical density (OD) of each well. The relative growth rate (RGR) for each group of cells was calculated using the following formula. The morphological changes and cytotoxicity of cells were evaluated according to GB/T 16 886 standards. For each cement group, five specimens were tested.

$$RGR = \frac{OD_T - OD_R}{OD_N - OD_R} \times 100\%$$

where OD_T is the optical density of the experimental group; OD_N is the optical density of the blank control group; OD_R is the optical density of the cell-free medium.

2.9 Determination of hemolysis rate

The experiment was performed at 24 °C ± 1 °C with a relative humidity of 40% ± 5%. According to the GB/T16886 standard, 1.8 mL of the above-prepared bone cement saline extract (see 2.3 for details) was placed in a sterile centrifuge tube for each group, 1.8 mL of purified water was used as a positive control, and 1.8 mL of normal saline was used as a negative control. To

each tube, 200 μL of 2% rabbit erythrocyte suspension was added. And then the tubes were incubated at 37 °C, 5% CO_2 for 1 h. Subsequently, the solution of each group was centrifuged at 3000 rpm for 5 min. The transparency of the supernatant was visually inspected to assess hemolysis. The optical density (OD) of the supernatant was measured at 545 nm using a microplate reader. Three samples ($n = 3$) were measured in each group of bone cement. The hemolysis rate (HR) was calculated according to the following formula:

$$HR = \frac{OD_T - OD_N}{OD_P - OD_N} \times 100\%$$

where OD_T in the formula is the optical density of the experimental solution, OD_N is the optical density of the negative control, and OD_P is the optical density of the positive control. According to GB/T 16 886, a hemolysis rate of less than 5% is considered hemolysis-free.

2.10 Acute toxicity in mice

Systemic toxicity was evaluated according to GB/T16886 criteria. Twenty C57 mice weighing in the range of 17–21 g were selected and divided into four groups of five mice in each group using block randomization (ISO 28640). Saline extract was injected intraperitoneally at a ratio of 50 mL kg^{-1} at 5 mm from the line of the lower abdomen of the mouse. Mice were housed in a ventilated and dry environment at 18–22 °C and given adequate food and water. The general condition and signs of toxicity of mice at 24, 48, and 72 hours after injection were observed. The weight changes of the mice were recorded. Mice were euthanized by neck dislocation at 72 h, and the liver and kidney were removed, sectioned, and stained with hematoxylin-eosin stain; the sections were observed under a microscope.

2.11 Determination of maximum polymerization temperature and setting time

Under the conditions of 24 °C ± 1 °C and 40% ± 5% relative humidity, 1 g of bone cement was filled into a mold to measure the polymerization temperature, and the temperature changes with time during the polymerization process were recorded using an infrared thermal imager. The real-time temperature was recorded every 15 s. The setting time (t_{set}) was calculated as the time at which T_{set} was achieved, with $T_{set} = (T_{max} + T_{amb})/2$, where T_{max} was the maximum temperature reached during the polymerization of the cement dough, and T_{amb} was the ambient temperature. For each cement group, three specimens were used.

2.12 Determination of injectability

As a bone substitute filling material, we evaluated the filling performance of bone cement. A 3D-printed vertebral model was filled with foam with rich gaps, followed by the injection of an appropriate amount of bone cement. After the bone cement is cured, excess foam on the surface was removed, and the morphology was observed. In addition, fresh porcine cadaver vertebrae were purchased, and surface muscles and soft tissues were removed. Cylindrical cavities with a diameter of 4 mm and a depth of 50 mm were drilled along the pedicle direction. Bone cement was injected into the cavities, and X-rays were taken.

2.13 Statistical analysis

Data were analyzed using SPSS 27.0 software, and the measured values are mean ± standard deviation. Antibacterial activity, compressive strength, elastic modulus, relative growth rate (RGR), hemolysis rate, coagulation time, radiopacity, and polymerization temperature were statistically analyzed using a non-parametric test (Kruskal–Wallis H test), followed by post-hoc analysis between groups using Dunn's test. Statistical significance was defined as a p-value of less than 0.05 ($p < 0.05$).

3. Results and discussion

3.1 Antibacterial activity

For clinical MRSA, AAEK1 demonstrated exceptional initial antibacterial performance: its inhibition zone width reached an impressive 13 mm on day 2, which was 2–6 times larger than those of the other two bone cements at the same time point (Fig. 2 and S1). Notably, after this initial burst release, although the antibacterial activity of AAEK1 bone cement gradually declined at subsequent time points, it maintained surprisingly stable and long-lasting antibacterial activity. Both AAEK2 and GS bone cements also exhibited burst drug release in the early stage, showing good antibacterial activity initially. However, their antibacterial effects gradually weakened over time, and the activity completely disappeared by day 3 or 4. Significant differences in antibacterial activity were observed between AAEK1 and GS bone cements at all time points ($p < 0.01$). AAEK2 showed comparable antibacterial activity to AAEK1 only on day 1 ($p > 0.05$), with significantly weaker performance at all other time points ($p < 0.01$). On days 1 and 2, no significant difference was found between AAEK2 and GS ($p > 0.05$), but GS exhibited a more pronounced decline in antibacterial activity over time ($p < 0.01$). Notably, the antibacterial activity of AAEK1 on day 7 was comparable to that of GS on day 1, highlighting its superior efficacy against drug-resistant bacteria, MRSA. Against *S. aureus*, the three cements showed similar early antibacterial activity, but AAEK2 and GS experienced a rapid decline over time (Fig. 2 and S2). By day 7, AAEK2-loaded bone cement exhibited almost no antibacterial activity, and the activity of GS dropped to a low level. In contrast, AAEK1 maintained stronger antibacterial activity than GS, with statistically significant differences in sustained efficacy compared to both AAEK2 and GS ($p < 0.01$). These results confirm that after the initial burst release, AAEK1 exhibits superior sustained antibacterial activity against both clinical MRSA and *S. aureus*. Although AAEK2 shows good initial activity, its long-term efficacy decreases significantly, similar to that of GS in the late stage. In addition, regarding the surface antibacterial activity of bone cement (see Fig. S7 for details), the surface antibacterial activity of the three bone cements on clinical MRSA decreased rapidly with time. Among them, gentamicin showed weak surface antibacterial activity in the early stage, which was significantly different from the other two types of bone cement ($p < 0.01$), which may be
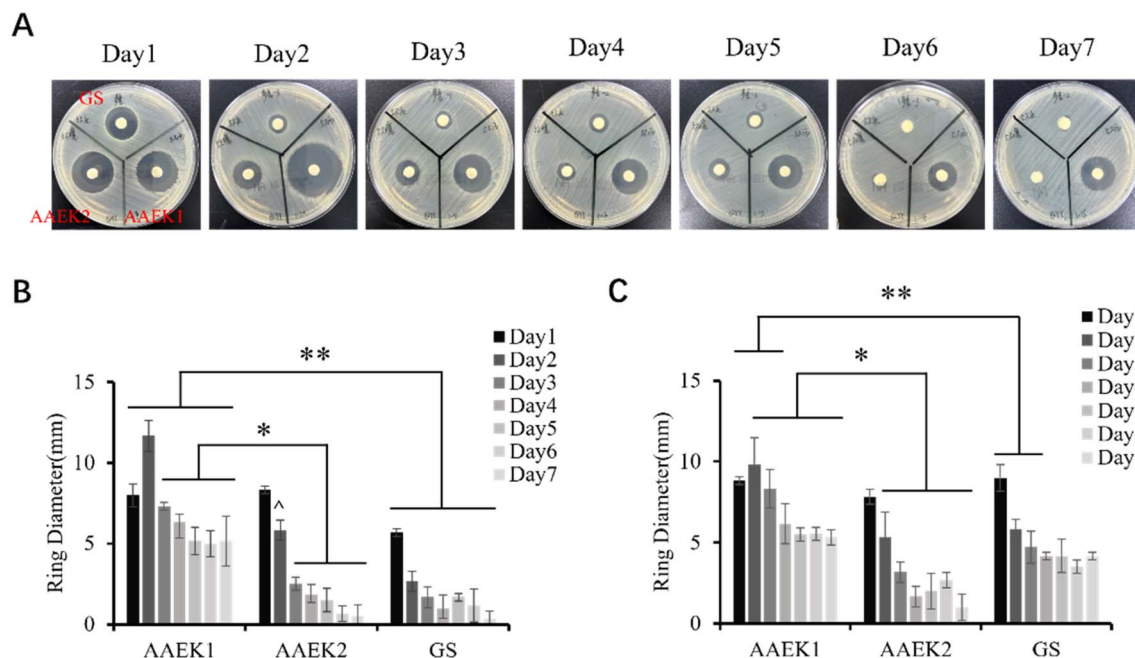
Fig. 2 Inhibition zones of 5 wt% AAEK1, 5 wt% AAEK2 and 5 wt% GS cement against clinical MRSA and *S. aureus*. (A) 7 days inhibition zones of three cements against clinical MRSA. (B) Ring diameter of the three cements against clinical MRSA (*: between AAEK1 and AAEK2 on days 3–7, $p < 0.01$; **: between AAEK1 and GS on days 1–7, $p < 0.01$; ^: compared to AAEK1, $p < 0.01$). (C) Ring diameters of the three cements against *S. aureus* (*: between AAEK1 and AAEK2 on days 2–7, $p < 0.01$; **: between AAEK1 and GS on days 1–3, $p < 0.01$).

related to the bacterial gentamicin–resistant properties and the heterogeneous release of the drug. The decrease in the antibacterial activity of AAEK1 and AAEK2 may be related to the explosive release of the drug, and it is not enough to provide sufficient antibacterial adhesion effect to reduce the surface antibacterial activity after the later release of the surface drug is complete. For *Staphylococcus aureus*, AAEK1 and gentamicin both showed excellent antibacterial activity in the later stage. The high antibacterial activity of gentamicin is undeniable, and the performance of AAEK1 may be related to the formation of drug release pathways.

3.2 Surface morphology

The results (Fig. 3A) revealed that the fracture section of the PMMA group exhibited negligible morphological changes before and after soaking. Notably, all three groups of bone cements—regardless of soaking—contained uniformly shaped oval pores, which originated from air entrapment during the polymerization process. In the AAEK1 group, the fracture section before soaking displayed numerous strip-like structures, representing the space-occupying crystal morphology of AAEK1 itself. Consequently, after soaking, the fracture section featured abundant elongated strip-like pores, presumably formed by the dissolution or extraction of AAEK1 drug clusters. After soaking, the GS bone cement also showed some circular voids, which may be formed after the elution of gentamicin drug clusters. Therefore, we used SEM to observe AAEK1 monomer (Fig. S4), and the AAEK1 monomer forms elongated crystals or strip-like structures, which may help enhance the

complete interconnectivity of the bone cement and promote the release of AAEK1 within the cement.[2] In contrast, for ALBC, the content of antibiotics need to reach 30–40% to achieve complete interconnectivity, thereby releasing the antibiotics inside the bone cement.[2] Therefore, this unique microstructure is likely the reason why SLBC containing AAEK1 can maintain antibacterial activity for a long time.

Fig. 3B displays the FT-IR spectra of two types of bone cements: PMMA and AAEK1. The two types of bone cement have the same peaks at 1150, 1244, 1730, and 2950 cm^{-1}, which is the characteristic peak of acrylic bone cement. The stretching vibration of O–CH_3 has a corresponding peak at 1150 cm^{-1}, while the asymmetric tensile vibration of C=O and C–H_2 has a corresponding peak at 1730 cm^{-1} and 2950 cm^{-1}, respectively. Additionally, in the infrared image of AAEK1, a tensile vibration peak belonging to the benzene ring appears at 1570 cm^{-1}, which is a unique structural peak of AAEK1, indicating that AAEK1 was successfully loaded into the bone cement.

3.3 Radiopacity

Fig. S6 shows the HU of the three types of bone cements (PMMA, AAEK1, and GS) scanned by CT at 120 vKp. The results showed that the cement exhibited good radiopacity with the addition of 10% $BaSO_4$. Bone cement that usually meets ISO 5833 standards and contains sufficient contrast agent usually has a HU range of greater than 2000 and may even be greater than 3000 under clinical CT scan conditions (tube voltage 120 kVp). With the addition of different antibacterial substances, the HU of the bone cement in this formula fluctuates slightly, with
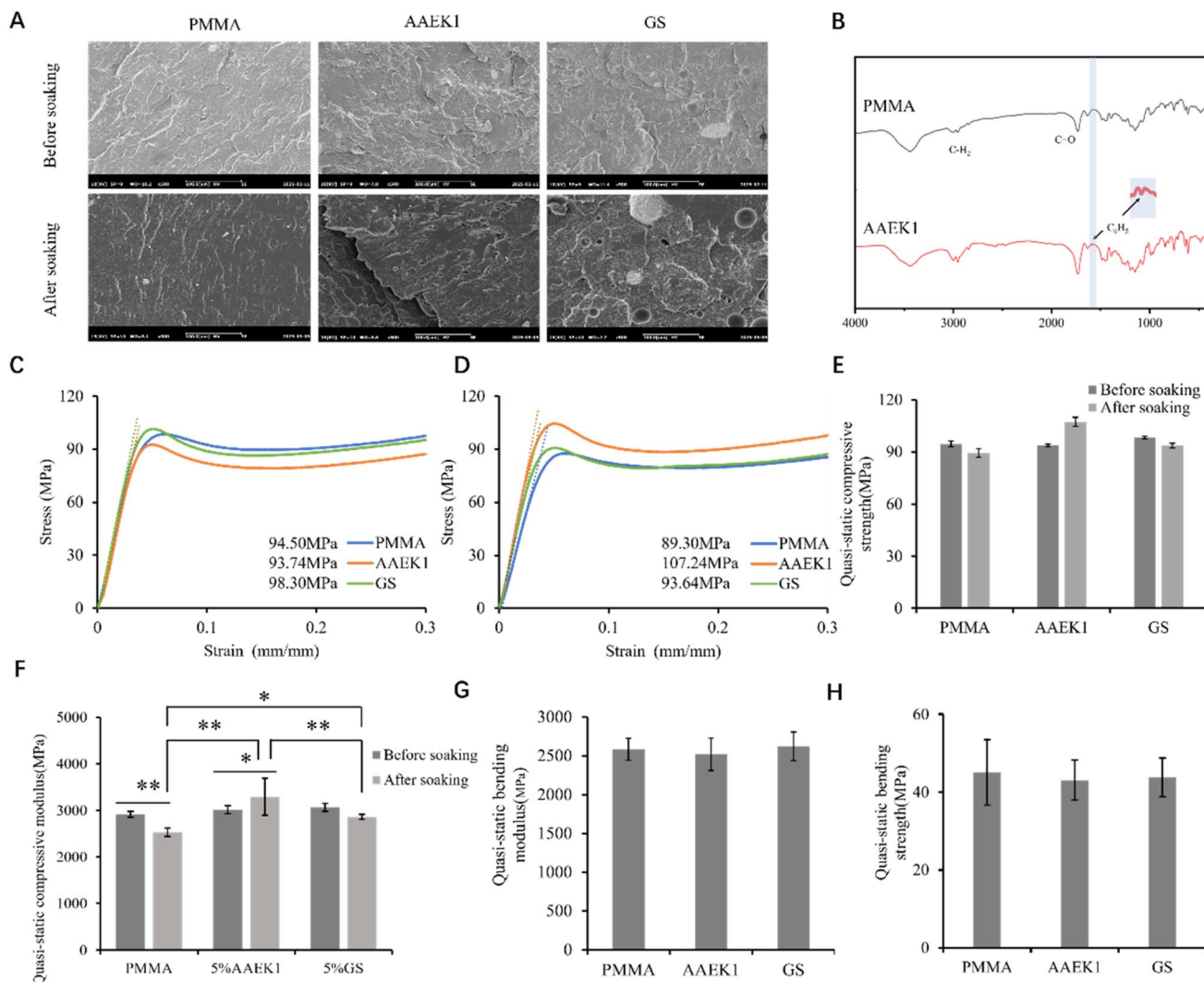
Fig. 3 Characterization and quasi-static compressive properties of PMMA, 5 wt% AAEK1, and 5 wt% GS cement. (A) SEM images of PMMA, AAEK1 and GS cement before and after 7 days of soaking. (B) FT-IR spectra of PMMA and AAEK1 cement. (C) Stress–strain curves of PMMA, AAEK1 and GS before soaking. (D) Stress–strain curves of PMMA, AAEK1 and GS cement after 7 days of soaking. (E) Quasi-static compressive strength of PMMA, AAEK1 and GS cement (*: $p < 0.01$ compared with the other two groups under the same treatment). (F) Quasi-static compressive modulus of PMMA, AAEK1 and GS cement (*: $p < 0.05$; **: $p < 0.01$). (G) Quasi-static bending modulus of PMMA, AAEK1 and GS cement. (H) Quasi-static bending strength of PMMA, AAEK1 and GS cement.

a significant difference between AAEK1 and GS ($p < 0.05$), which may be caused by the added antibacterial substances, but the bone cement still meets the standard requirements for clinical use.

3.4 Quasi-static compressive strength and modulus

Fig. 3C–F present the stress–strain curves and quasi-static mechanical strength of PMMA, AAEK1, and GS cements before and after 7 days soaking. The stress–strain curves were analyzed by calculating the quasi-static elastic modulus from the linear slope and defining the yield strength as the quasi-static compressive strength. Notably, only AAEK1 cement exhibited a significant increase in mechanical strength after soaking ($p < 0.01$), while the other two cements showed varying degrees of strength reduction with no statistical significance (p

> 0.05). Before soaking, no significant differences in mechanical strength were observed among the three groups. After 7 days of soaking, AAEK1 cement demonstrated the highest mechanical strength, with significant differences from the other two groups ($p < 0.01$). The quasi-static elastic modulus of the three types of bone cements is different. The elastic modulus of PMMA ($p < 0.01$) and gentamicin bone cement decreased after soaking, while that of AAEK1 increased ($p < 0.05$), which was the same as the change trend observed for quasi-static compressive strength. Significant differences in elastic modulus were found among the three types of soaked bone cements ($p < 0.05$), and this change in mechanical properties may be related to the drug structure and dissolution residual pores (which formed after the elution of drug clusters). Importantly, the mechanical strength of both antibacterial bone cements (AAEK1 and GS)

met the international standard (ISO 5833) for clinical use, which requires a compressive strength of >70 MPa, both before and after soaking. In addition, results from the three-point bending experiment (Fig. 3G and H) showed that the addition of antibacterials did not significantly reduce the quasi-static bending strength of bone cement, and the bending modulus was in line with the ISO5833 specification of ≥1800 MPa, with no significant difference among the three.

3.5 Cytotoxicity (CCK-8)

Fig. 4A illustrates the cytotoxicity results of various cements on MC3T3-E1 cells. As per GB/T 16886 standards, 5 wt% GS cement exhibited no obvious cytotoxicity. Notably, 5 wt% AAEK1 bone cement showed a relative growth rate (RGR) of <75% on day 3, indicating mild cytotoxicity. This phenomenon may be attributed to drug-induced damage to the cell membrane or the burst release of high drug concentrations during the early stage, though no significant cytotoxicity was observed at other time points. Given the cytotoxicity observed with 5 wt% AAEK1, additional CCK-8 assays were performed using low-dose AAEK1 bone cements (1.25 wt% and 2.5 wt%). The results (Fig. S5A) showed that both low-dose groups maintained RGR values above the 75% threshold, confirming no significant cytotoxicity. This further suggests that cell damage was likely associated with the high-concentration drug release from the 5 wt% formulation. Overall, AAEK1 cement exhibits low cytotoxicity and shows great potential for application. As CCK-8 assays alone cannot fully characterize the biocompatibility of AAEK1, we extended our analysis to include *in vitro* hemolysis experiments and *in vivo* acute toxicity tests in mice.

3.6 *In vitro* hemolysis

As shown in Fig. 4B, no hemolysis was observed in the supernatant of any bone cement group. The hemolysis rates of 5 wt% AAEK1 and 5 wt% GS cements were evaluated, with statistical analysis showing that the hemolysis rates of each group were <5% and no significant differences were found ($p > 0.05$). This indicates that both antibacterial bone cements do not cause hemolysis of rabbit erythrocytes. In line with the CCK-8 experimental results, hemolysis experiments were also conducted on

two groups of low-dose AAEK1 cements (1.25 wt% and 2.5 wt%). The results (Fig. S5B) showed that low-dose AAEK1 cements exhibited no significant hemolytic toxicity, with hemolysis rates not significantly different from the control group ($p > 0.05$). Based on the findings of the two biocompatibility experiments above, antibacterial activity tests were additionally performed on two groups of low-dose AAEK1 bone cements against clinical MRSA. The results demonstrated that both low-dose groups still exhibited excellent anti-drug resistance activity (Fig. S5C).

3.7 Acute toxicity in mice

After intraperitoneal injection of the extract, all mice exhibited normal behavior, with no toxic manifestations such as dyspnea, hypoactivity, diarrhea, or vomiting observed at 24 hours, 48 hours, and 72 hours after intraperitoneal injection. Body weight changes during the rearing period are presented in Table S2. In Fig. 5, histological analysis of liver sections revealed that after injection of the extract, liver lobules maintained intact morphology, hepatocytes showed normal structure, and no obvious hyperemia or inflammatory cell infiltration was observed in the confluence areas. Compared with the saline group, mouse hepatocytes displayed no significant swelling, degeneration, or necrosis. For renal observations, the morphological structure of the renal cortex and medullary cells in each group was normal. Glomeruli and renal tubules showed no obvious abnormalities, with no edema, necrosis, or shedding of tubular epithelial cells. Additionally, no obvious inflammatory cell infiltration was detected in the renal mesenchyme. Therefore, the test results show that AAEK1 cement does not induce acute toxicity in mice.

3.8 Maximum polymerization and setting time

As shown in Fig. 6A, the temperature profile during the polymerization of 5 wt% AAEK1 cement is depicted. The incorporation of GS and AAEK1 did not significantly impact the exothermic behavior of the polymerization reaction (Fig. 6B). The maximum polymerization temperature recorded for all three cements fluctuated between 63 °C and 65 °C, with no statistically significant differences observed ($p > 0.05$). For the setting time assessment (Fig. 6C), all cements exhibited setting
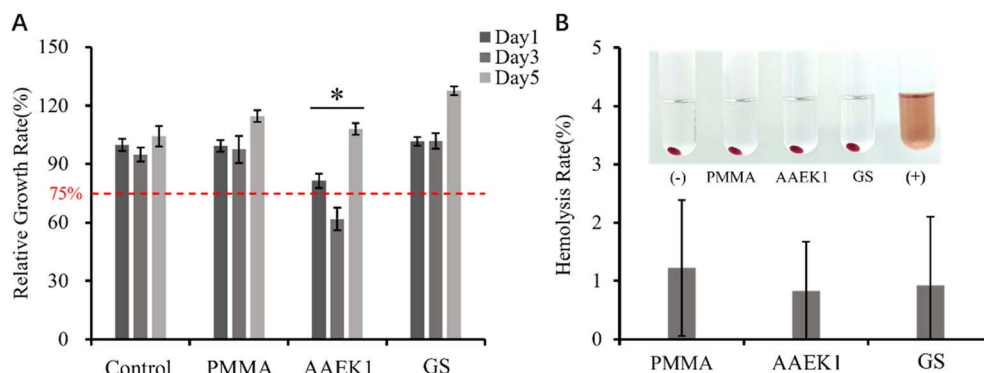

Fig. 4 CCK-8 and hemolysis experiments of PMMA, 5 wt% AAEK1 and 5 wt% GS cement. (A) Relative growth rate (RGR) of the three types of bone cements at different time points (*: $p < 0.01$). (B) Hemolytic activity of the three types of bone cements and the corresponding visual views.
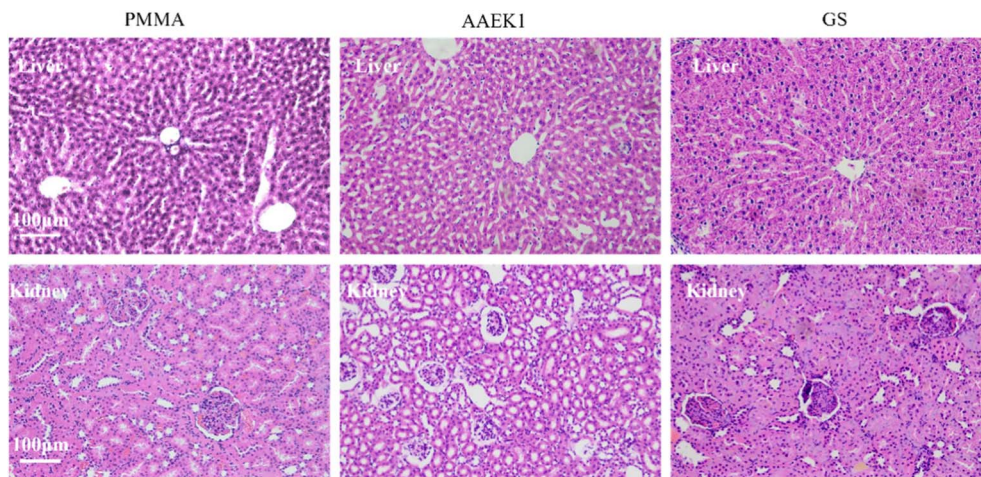
Fig. 5 Histological staining of mouse liver and kidney 3 days after intraperitoneal injection of bone cement extracts, observed under a light microscope.

times ranging from 135 to 180 seconds, as calculated by the established formula, with no significant intergroup differences ($p > 0.05$). It is important to emphasize that the experimental formulation in this study still requires further optimization to achieve a setting time of 5–15 minutes, so that it can meet the requirements for clinical application.

3.9 Injectability

ALBC is most commonly used for the prevention and treatment of PJI, and it may also be applied in spinal surgeries. Therefore, it is necessary to investigate whether the addition of AAEK1 affects the properties such as the injectability, fillability, and anti-leakage capability of cement. Therefore, from an application perspective, we evaluated these properties of bone cement using two models: a 3D-printed human vertebral body model
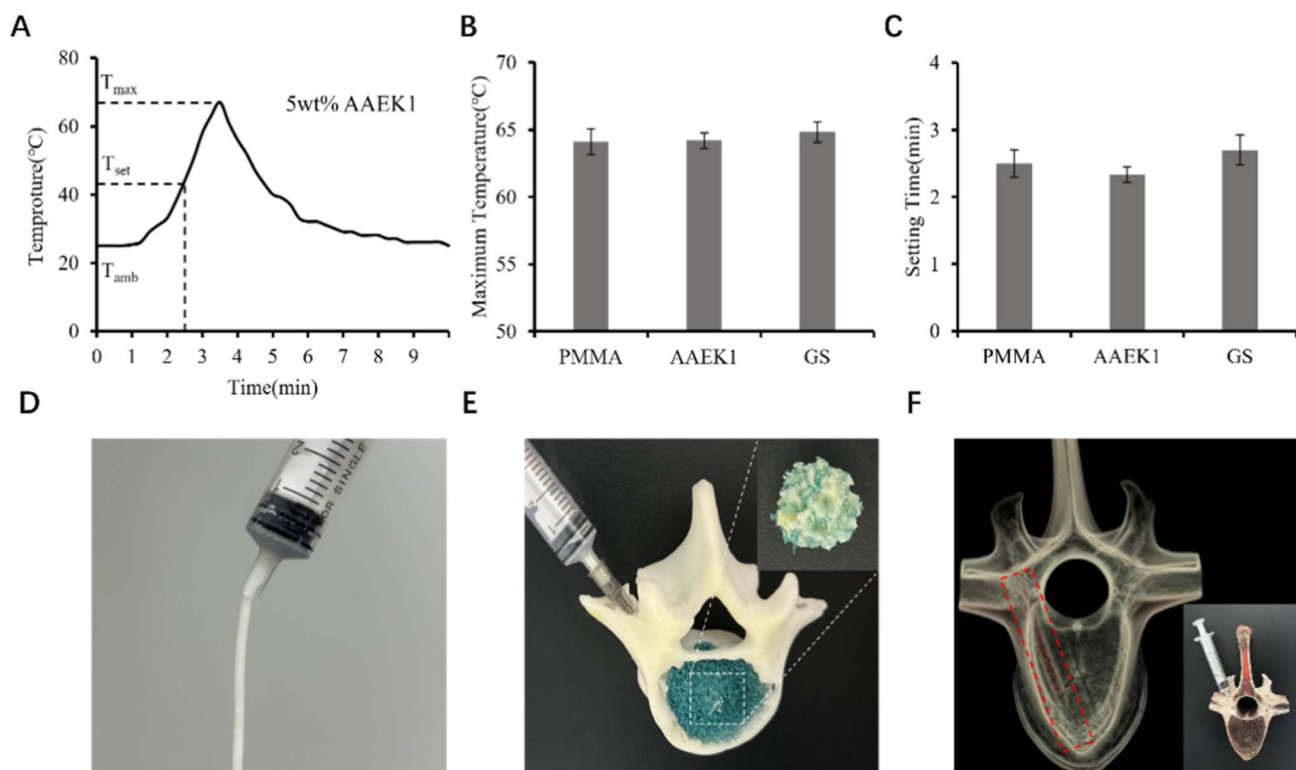

Fig. 6 Polymerization temperature, setting time, and operability of cement. (A) Polymerization temperature curve over time for 5 wt% AAEK1 cement. (B and C) Maximum polymerization temperature and setting time of PMMA, AAEK1 and GS cements. (D) Injectability of AAEK1 cement. (E) Evaluation of the filling and diffusion properties of AAEK1 cement in a 3D-printed human vertebral body model. (F) X-ray image after injection of AAEK1 cement.

and porcine vertebrae. As shown in Fig. 6D, AAEK1 bone cement demonstrated excellent injection performance. When injected into the 3D vertebral model filled with foam, the cement exhibited an elliptical distribution within the model after removing the surface foam—evidence of its superior filling capacity and a low risk of leakage (Fig. 6E). Furthermore, X-ray imaging of porcine vertebrae after cavity injection showed uniform distribution of the bone cement, further confirming the exceptional injectability and fillability of AAEK1 (Fig. 6F).

3.10 Limitations

(1) This study did not use vacuum mixing technology, which may undermine the credibility of the entire study.

(2) The drug elution of SLBC is similar to that of ALBC, so they are ineffective against the formation of biofilm on the implant surface.

(3) Fatigue life and fatigue creep propagation resistance were not included in this study, which reduces its clinical relevance.

(4) This study preliminarily proposes that the sortase A inhibitor formulation is superior to the gentamicin formulation in combating MRSA; however, it is unlikely that this study and its results will inform choices made in clinical practice involving cemented TJR.

4 Conclusions

We formulated a sortase A inhibitor (AAEK1)-loaded PMMA bone cement (SLBC) that targets MRSA. Compared with a laboratory-prepared gentamicin-loaded bone cement, SLBC showed significantly higher activity against MRSA and prolonged anti-MRSA activity. SLBC meets the ISO5833 standard in terms of quasi-static compressive strength, maximum polymerization temperature, and setting time, and the cement showed excellent biocompatibility *in vivo* and *in vitro* tests and high injectability. These findings suggest that SLBC may have potential for the management and treatment of PJI in TJI and, as such, deserves further study.

Ethics statement

The animal study was conducted with approval from the Biomedical Ethics Committee of Hefei University of Technology (No. HFUT20241025-002) and complied with the National Institutes of Health Guide for the Care and Use of Laboratory Animals. This study was conducted in accordance with the declaration of Helsinki.

Author contributions

Conception and design of the research: Yang Xu, Jian-Jun Chu. Acquisition of data: Yin-Yu Qin, Lu-Yang Han, Long-Xu Han, Wen-Han Bu, Shu-Yi Cheng, Chen Wang. Analysis and interpretation of the data: Yin-Yu Qin, Yang Xu. Statistical analysis: Yin-Yu Qin, Yang Xu. Obtaining financing: Jian-Jun Chu, Yang Xu. Writing of the manuscript: Yin-Yu Qin, Yang Xu. Critical revision of the manuscript for intellectual content: Yang Xu, Jian-Jun Chu.

Conflicts of interest

The authors declare that the research was conducted in the absence of any commercial or financial relationships that could be construed as a potential conflict of interest.

Data availability

The original contributions presented in the study are included in the article/SI; further inquiries can be directed to the corresponding author. See DOI: **https://doi.org/10.1039/d5ra04437e**.

Acknowledgements

References

1 H. Lin, Z. Gao, T. Shan, A. Asilebieke, R. Guo, Y. C. Kan, C. Li, Y. Xu and J. J. Chu, *J. Orthop. Surg. Res.*, 2024, **19**(1), 673.

2 V. J. Suhardi, D. A. Bichara, S. Kwok, A. A. Freiberg, H. Rubash, H. Malchau, S. H. Yun, O. K. Muratoglu and E. Oral, *Nat. Biomed. Eng.*, 2017, **1**, 0080.

3 H. Tesfaye Leta, S. A. Lie, A. M. Fenstad, S. H. L. Lygre, M. Lindberg-Larsen, A. B. Pedersen, A. W-Dahl, O. Rolfson, E. Bülow, L. N. van Steenbergen, R. G. H. H. Nelissen, D. Harries, R. de Steiger, O. Lutro, K. Mäkelä, M. S. Venäläinen, J. Willis, M. Wyatt, C. Frampton, A. Grimberg, A. Steinbrück, Y. Wu, C. Armaroli, M. A. Gentilini, R. Picus, M. Bonetti, S. Dragosloveanu, A. E. Vorovenci, D. Dragomirescu, H. Dale, C. Brand, B. Christen, J. Shapiro, J. M. Wilkinson, R. Armstrong, K. Wooster, G. Hallan, J.-E. Gjertsen, R. N. Chang, H. A. Prentice, A. Sedrakyan, E. W. Paxton and O. Furnes, *JAMA Netw. Open*, 2024, **7**(5), e2412898.

4 H. Tesfaye Leta, A. M. Fenstad, S. H. L. Lygre, S. A. Lie, M. Lindberg-Larsen, A. B. Pedersen, A. W-Dahl, O. Rolfson, E. Bülow, J. A. Ashforth, L. N. van Steenbergen, R. G. H. H. Nelissen, D. Harries, R. de Steiger, O. Lutro, E. Hakulinen, K. Mäkelä, J. Willis, M. Wyatt, C. Frampton, A. Grimberg, A. Steinbrück, Y. Wu, C. Armaroli, M. Molinari, R. Picus, K. Mullen, R. Illgen, I. C. Stoica, A. E. Vorovenci, D. Dragomirescu, H. Dale, C. Brand, B. Christen, J. Shapiro, J. M. Wilkinson, R. Armstrong, K. Wooster, G. Hallan, J.-E. Gjertsen, R. N. Chang,

H. A. Prentice, E. W. Paxton and O. Furnes, *Acta. Orthop.*, 2023, **94**, 416–425.

5 J. Singh, J. B. Mandell, J. Scheidt, J. D. Orlando, J. C. Kadir, W. B. Ribnick, K. M. Brothers, K. L. Urish and S. A. Sydlik, *Adv. Funct. Mater.*, 2024, **35**, 2406126.

6 E. L. Cyphert, G. D. Learn, S. K. Hurley, C. Y. Lu and H. A. von Recum, *Adv. Healthc. Mater.*, 2018, **7**(21), e1800812.

7 Y. Xu, H. Lin, Z. Gao, R. Guo, Y.-c. Kan, L.-y. Han, W.-h. Bu, Z. Wang, A. Asilebieke, L.-x. Han, C. Li, F. He and J. J. Chu, *J. Mater. Chem. B*, 2024, **12**, 4389–4397.

8 Z. Gao, Y. Xu, Y. Kan, H. Li, R. Guo, L. Y. Han, W. H. Bu and J. J. Chu, *J. Orthop. Surg. Res.*, 2023, **18**(1), 569.

9 L. Chen, Y. F. Tang, K. Zha, X. Zha, M. Wei, Q. C. Tan and Z. X. Wu, *J. Mater. Chem. B*, 2020, **9**, 508–522.

10 Y. Al Thaher, R. Khalil, S. Abdelghany and M. S. Salem, *Nanomaterials*, 2022, **12**, 1381.

11 M. M. Farhan-Alanie, H. G. Burnand and M. R. Whitehouse, *Bone Joint J.*, 2021, **103B**, 7–15.

12 S. Mistry, R. Roy, A. K. Jha, N. Pandit, S. Das, S. Burman and M. Joy, *J. Contr. Release*, 2022, **346**, 180–192.

13 Y. Zhao, G. K. Mannala, R. Youf, M. Rupp, V. Alt and M. Riool, *Antibiotics*, 2024, **13**, 692.

14 S. Ghosh, M. Sinha, R. Samanta, S. Sadhasivam, A. Bhattacharyya, A. Nandy, S. Saini, N. Tandon, H. Singh, S. Gupta, A. Chauhan, K. K. Aavula, S. S. Varghese, P. Shi, S. Ghosh, M. K. Garg, T. Saha, A. Padhye, S. Ghosh, H. L. Jang and S. Sengupta, *Nat. Biomed. Eng.*, 2022, **6**, 1180–1195.

15 D. R. Long, A. Cifu, S. J. Salipante, R. G. Sawyer, K. Machutta and J. C. Alverdy, *JAMA Surg.*, 2024, **159**, 949–956.

16 M. Verma, S. Randhawa, M. Bathla, N. Teji and A. Acharya, *J. Mater. Chem. B*, 2025, **13**, 4770–4790.

17 G. Lewis, *World J. Orthop.*, 2022, **13**, 339–353.

18 F. Shatila, T. Yalçın and İ. Yaşa, *Acta Biologica Turcica*, 2019, **32**, 220–235.

19 B. Zhang, Y. F. Tang, F. Liang, H. Zhang, Y. N. Sun, L. Chen, C. Y. Chen, Y. M. Zhang, X. F. Hu, K. Zhao and Z. X. Wu, *Chem. Eng. J.*, 2025, **516**, 163902.

20 C. E. Heim, M. E. Bosch, K. J. Yamada, A. L. Aldrich, S. S. Chaudhari, D. Klinkebiel, C. M. Gries, A. A. Alqarzaee, Y. X. Li, V. C. Thomas, E. Seto, A. R. Karpf and T. Kielian, *J. Immunol.*, 2021, **206**, 110–119.

21 F. Valour, O. Miot, C. Batailler, S. Goutelle and T. Ferry, *Clin. Microbiol. Infect.*, 2025, 00184–3.

22 X. N. Guan, T. Zhang, T. Yang, Z. Dong, S. Yang, L. F. Lan, J. H. Gan and C. G. Yang, *RSC Med. Chem.*, 2021, **13**, 138–149.

23 R. Sapra, A. K. Rajora, P. Kumar, G. P. Maurya, N. Pant and V. Haridas, *J. Med. Chem.*, 2021, **64**, 13097–13130.

24 A. Touati, N. A. Ibrahim and T. Idres, *Pathogens*, 2025, **14**, 386.

25 L. Wang, G. Wang, H. Qu, K. Wang, S. Jing, S. Guan, L. Su, Q. Li and D. Wang, *Front. Microbiol.*, 2021, **12**, 686864.

26 W. Song, L. Wang, Y. Zhao, G. Lanzi, X. Wang, C. Zhang, J. Guan, W. Wang, X. Guo, Y. Meng, B. Wang and Y. Zhao, *Microbiol. Spectr.*, 2022, **10**(4), 1–13.

27 H. Abujubara, J. C. J. Hintzen, S. Rahimi, I. Mijakovic, D. Tietze and A. A. Tietze, *Chem. Sci.*, 2023, **14**(25), 6975–6985.

28 S. Cascioferro, D. Raffa, B. Maggio, M. V. Raimondi, D. Schillaci and G. Daidone, *J. Med. Chem.*, 2015, **58**, 9108–9123.

29 S. Alharthi, S. E. Alavi, P. M. Moyle and Z. M. Ziora, *Drug Discov. Today*, 2021, **26**, 2164–2172.

30 J. Zhang, H. Liu, K. Zhu, S. Gong, S. Dramsi, Y. T. Wang, J. Li, F. Chen, R. Zhang, L. Zhou, L. Lan, H. Jiang, O. Schneewind, C. Luo and C. G. Yang, *Proc. Natl. Acad. Sci. U. S. A.*, 2014, **111**, 13517–13522.

31 A. W. Maresso, R. Wu, J. W. Kern, R. Zhang, D. Janik, D. M. Missiakas, M. E. Duban, A. Joachimiak and O. Schneewind, *J. Biol. Chem.*, 2007, **282**, 23129–23139.

32 Z. Gao, Y. C. Kan, Y. H. Xie, R. Guo, C. Li, A. Asilebieke, Y. Xu and J. J. Chu, *Aip Adv.*, 2023, **13**, 105034.

33 D. Neut, H. van de Belt, J. R. van Horn, H. C. van der Mei and H. J. Busscher, *Acta Orthop. Scand.*, 2003, **74**, 670–676.

34 S. P. von Hertzberg-Boelch, M. Luedemann, M. Rudert and A. F. Steinert, *Biomedicines*, 2022, **10**(8), 1830.